RIS-Assisted Passive Localization (RAPL): An Efficient Zero-Overhead Framework Using Conditional Sample Mean

Jiawei Yao, Yijie Mao, *Member, IEEE*, Mingzhe Chen, *Senior Member, IEEE*, Ye Hu, *Member, IEEE*

***Abstract*—Reconfigurable Intelligent Surface (RIS) has been recognized as a promising solution for enhancing localization accuracy. Traditional RIS-based localization methods typically rely on prior channel knowledge, beam scanning, and pilot-based assistance. These approaches often result in substantial energy and computational overhead, and require real-time coordination between the base station (BS) and the RIS. To address these challenges, in this work, we move beyond conventional methods and introduce a novel data-driven, multiple RISs-assisted passive localization approach (RAPL). The proposed method includes two stages, the angle-of-directions (AoDs) between the RISs and the user is estimated by using the conditional sample mean in the first stage, and then the user's position is determined based on the estimated multiple AoD pairs in the second stage. This approach only utilizes the existing communication signals between the user and the BS, relying solely on the measurement of received signal power at each BS antenna for a set of randomly generated phase shifts across all RISs. Moreover, by obviating the need for real-time RIS phase shift optimization or user-to-BS pilot transmissions, the method introduces no additional communication overhead, making it highly suitable for deployment in real-world networks. The proposed scheme is then extended to multi-RIS scenarios considering both parallel and cascaded RIS topologies. Numerical results show that the proposed RAPL improves localization accuracy while significantly reducing energy and signaling overhead compared to conventional methods.**

***Index Terms*—Reconfigurable intelligent surface (RIS), localization, conditional sample mean, discrete phase shift.**

I. Introduction

With the development of industrial Internet of Things (IIoT), intelligent vehicles, and robot technologies, the availability, accuracy and timeliness of localization data have become particularly important [1]. The 3rd Generation Partnership Project (3GPP) has made significant advancements in standardizing localization features for modern wireless networks. This integration facilitates radio localization, aiming to achieve high-precision location accuracy by utilizing radio frequency (RF) and adaptive numerology within the physical layer [1], [2]. Radio localization typically relies on parameters like time-of-arrival (ToA), received signal strength (RSS), and angular information, such as angle-of-arrival (AoA). Specifically, ToA measurements can enhance localization accuracy, but they demand precise synchronization across anchors, adding extra overhead. RSS-based localization methods have widely applied in indoor localization, and their performance can be potentially affected by large errors in multipath environments. [3]. Localization based on angular information, which provides the geometric relationship between transceivers, has also been widely used to pinpoint the position of a target. For example, [4]–[6] explore the use of large-scale antenna arrays to estimate the angle-of-arrival (AoA) at the base station (BS). In addition, deploying more anchor points or access points (APs) in the networks is an effective way to improve the localization performance [7], but this approach leads to much higher energy consumption.

Reconfigurable intelligent surface (RIS), as known as intelligent reflecting surface (IRS), is a promising wireless technology that aims to reconstruct the wireless environment and enhance network performance by manipulating signal reflections [8]–[12]. RIS consists of numerous reflective elements (REs), allowing it to perform a similar function to large-scale antenna arrays by collecting ample directional information at a lower hardware cost [13]–[17]. Additionally, the extra reflective links enabled by RIS can further enhance beamforming gain and reduce energy consumption [18]. Owing to its appealing advantages, RIS can replace the small BSs and relays in future networks, and provide substantial improvements in throughput [19]–[21], coverage [22]–[24], reliability [25]–[28], and connectivity [29]. Recently, RIS has gained attention as a promising approach enhancing sensing and localization. The deployment of multiple RISs within the network further enhances communication and sensing performance [30]–[32], and provide much more directional information [33]–[35].

Most of existing works on RIS-assisted sensing, localization, and integrated sensing and communications (ISACs) focus on optimizing the Cramér-Rao lower bound (CRLB) [15], [35]–[40] or beam pattern gain [18], [41] to design waveforms, thereby enhancing the sensing performance. The angular or position information are then obtained by minimize mean squar error (MMSE) and multiple signal classification (MUSIC) algorithms. However, these methods heavily rely on the prior acquisitions of channel state information (CSI). In [15], the authors study a CRLB minimization problem in an uniform linear array (ULA) IRS-assisted ISAC system, the alternating optimization (AO), semi-definite relaxation (SDR), and successive convex approximation (SCA) are applied, the

J. Yao and Y. Mao are with the School of Information Science and Technology, ShanghaiTech University, Shanghai 201210, China (Email: jiaweiyao@link.cuhk.edu.cn, maoyj@shanghaitech.edu.cn).

M. Chen is with the Department of Electrical and Computer Engineering and Frost Institute for Data Science and Computing, University of Miami, Coral Gables, FL, 33146, USA (Email: mingzhe.chen@miami.edu).

Y. H is with the Department of Industrial and Systems Engineering, , University of Miami, Coral Gables, FL, 33146, USA (Email: yehu@miami.edu).

(Corresponding Author: Yijie Mao)

angle of direction (AoD) from IRS to the target is confirmed by MMSE method. However, within current 5G network, acquiring CSI in RIS-assisted wireless systems, notably in multi-RIS cases, presents many obstacles due to the passive nature of the REs at RIS, which limits direct control over the signal transmission and reception, making it difficult to obtain accurate and timely CSI. Additionally, prevailing channel estimation strategies entail communication interruptions, extra pilot overhead, and substantial interaction between the BS and the RIS [42]–[46].

Beam scanning-based methods also have widely applied to RIS-assisted sensing or localization. In [13], the authors consider a RIS-assisted multi-target sensing system, the RIS space-time beamforming is designed to improve the sensing resolution that is obtained by the decomposition of the channels. In [14], the authors propose a RIS-assisted beam scanning schemes with beam-squint and beam-split to obtain the angular information of users. By modifying the reflection coefficient of the RIS, the differences between the RSS values of adjacent locations can be enlarged. Based on this, the authors in [16] proposed a localization scheme by dynamically configuring phase shifts of the RIS and employing the maximum likelihood estimation. A multi-RIS-assisted sensing system is considered in [34], the authors model the wireless environment as a point cloud, and propose an atomic norm minimization (ANM)-based algorithm to detect the direction of each point. Whereas, it is worth noting that the beam scanning approaches employed in [14], [16], [34] are all mainly based on spatial beam scanning. Consequently, when applied to very large regions, these methods incur prohibitive errors or costs, thereby considerably narrowing their practical range of applicability. Additionally, the strong interactions between the BS, RISs and the user are still existed.

Moreover, a series of active sensing and localization approaches based on deep learning technologies are also widely investigated in [33], [47]–[50]. These approaches mainly rely on RSS information and use neural networks to extract key angular and position information. The authors in [33], [50] consider an uplink localization problem in multiple RISs-assisted multiple-input single-output (MISO) network. They propose two learning-based localization approaches, recurrent neural network (RNN)-based approach and deep neural network (DNN)-based approach. The RNN-based method makes use of RNN with long short term memory (LSTM) units to extract temporal features, e.g., current RSS information at the BS, phase shifts at the RISs. The DNN-based method makes use of DNN to extract features based on the prior channel distribution. After training with large amount of data, the BS can localize the user with a short pilot sequence by the two approaches. Even though they similarly dispense with the need for CSI acquisition, the communication disruption, strong interactions between devices and extra pilot overhead remain unavoidable. In addition, it is also difficult to obtain the extremely large amount of offline communication and sensing data required to train neural networks in practice. To put it in a nutshell, the limitations of existing localization methods are summarized as follows:

- ***Need for CSI Acquisition*:** The waveform design-based methods heavily rely on the CSI acquisition [13], [15], [18], [35]–[39], [41]. However, the CSI acquisition are challenging in a real multiple RISs-assisted network.
- ***Communication Interruptions*:** The pilots-assisted methods result in normal communication interruptions due to the pilots transmission and reception [33], [34], [36], [50].
- ***Strong Interactions*:** Some localization approaches need strong interactions between the devices for beam scanning [16], channel estimation [42]–[45], and timely data feedback [33], [50], which is not compatible with the current 5G protocol and lead to additional spectrum and energy overhead.
- ***Large Amounts of Training Data*:** The learning-based approaches need great amounts of data to training the neural networks [33], [47]–[50]. The acquisition of large amounts of training data is challenging in real environment, and it also leads extra computation source and energy overhead, which is incompatible for future IoT and edge networks.

Recently, in communication-only networks, the authors in [22], [32], [51]–[53] proposed a series of practical and data-driven approaches without the need of CSI, namely blind beamforming. These approaches use a set of random phase shift samples to configure the RIS and employs a blind feedback method, utilizing received signal power measurements to calculate the conditional sample mean. The conditional sample mean is a statistical method that computes the average received signal power, conditioned on the available information about the RIS phase shifts. Inspired by this approach, we propose a novel RIS-assisted passive localization approach to tackle the aforementioned limitations of existing localization approaches. The main novelties and advantages of our proposed localization approach, are summarized in the following:

1) We propose a novel RIS-assisted passive localization approach (RAPL) that leverages existing communication signals and the conditional sample mean method to achieve precise localization without incurring additional communication costs. In the first stage, the AoD pairs from each RIS to the user are estimated using the conditional sample mean approach. In the second stage, the user's position is determined based on the estimated AoD pairs. Throughout the process, only the received signal power measurements at each base station (BS) antenna are required. This approach effectively addresses the limitations of conventional localization methods by eliminating the need for CSI acquisition, preventing communication interruptions, minimizing interactions between the RISs and the BS, and eliminating the requirement for extensive training data. As a result, it is a zero-overhead approach and more easily deployable in future industrial IoT applications and diverse edge networks.
2) We further extend the proposed RAPL to a multiple RIS-assisted network, considering two distinct RIS topologies: the parallel topology, where each RIS reflects signals independently, and the cascaded topology, where RISs reflect signals sequentially. Compared to existing multiple RIS-assisted localization models, the two cases we

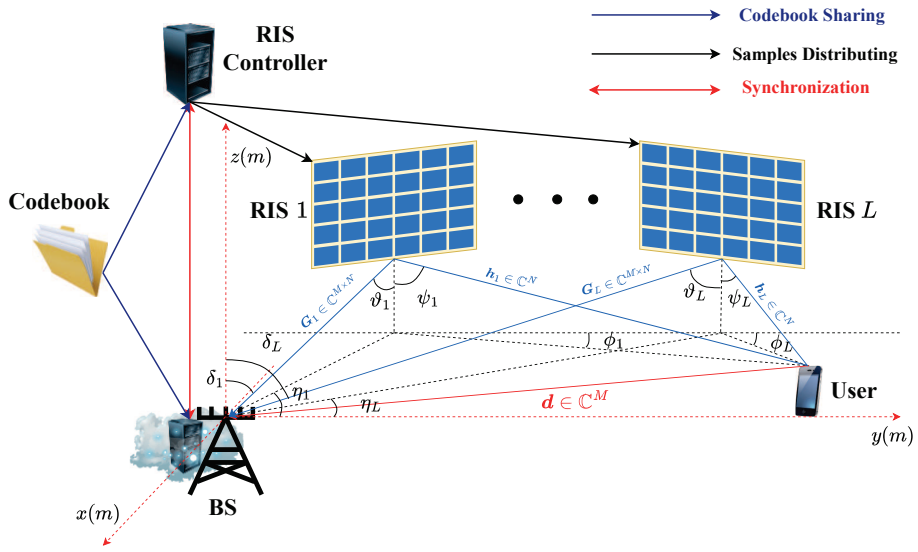

Fig. 1: Multiple RISs-assisted MISO network.

explore offer higher generalizability, which has not been addressed in previous studies.

3) Extensive numerical simulations are conducted to evaluate the performance of the proposed localization approach in various scenarios. The results demonstrate that, with the same number of training samples, the localization accuracy of the proposed algorithm is significantly higher than the benchmarks, especially under the constraint of discrete phase shifts. Moreover, the numerical results also show that the proposed RAPL attains excellent localization accuracy especially in the presence of cascaded channels, aligning closely with real-world environments.

The remaining paper is organized as follows. Section II presents the system model and problem statement. In Section III, we discuss the proposed RAPL–AoD estimation approach. Section IV extends the approach to the multi-RIS cases and elaborate that how to pinpoint the user position based on the AoD pairs, followed by numerical evaluations in Section V. Finally, conclusions are drawn in Section VI.

The notation here and throughout is summarized as follows. We use a, $\boldsymbol{a}$, $\boldsymbol{A}$ to denote scalar, vector, matrix respectively. $\boldsymbol{A}^\top$ and $\boldsymbol{A}^\mathsf{H}$ to denote transpose and Hermitian, $|\mathcal{A}|$ to denote the cardinality of the set $\mathcal{A}$, $[\boldsymbol{a}]_j$ to denote the jth element of the vector $\boldsymbol{a}$, and $[\boldsymbol{A}]_{i,j}$ to denote the (i,j)th element of the matrix $\boldsymbol{A}$. We use $\mathrm{diag}(\boldsymbol{a})$ to denote the diagonal matrix with entries of $\boldsymbol{a}$ on the diagonal, $\mathrm{tr}(\cdot)$ to denote the trace of a square matrix. We use $\mathcal{CN}(\cdot,\cdot)$ to denote a complex Gaussian distribution; $\mathbb{E}(\cdot)$ to denote the expectation of a random variable. We use $\lfloor\cdot\rfloor$ to denote the floor function and $\mathrm{mod}(\cdot)$ to denote the modulo division. Moreover, the argument of a complex number is written as $\angle(\cdot)$, and the discrete set $\{a, a+1, \ldots, b-1, b\}$ is written as $[a:b]$ for two integers $a < b$.

II. System Model and Problem Statement

A. Channel Model

Consider an uplink indoor localization task where a BS equipped with M transmit antennas aims to determine the location $\boldsymbol{p} = (x, y, z)$ of a single-antenna user with the assistance of multiple RISs, as illustrated in Fig. 1. L planar RISs are deployed in the network, and we use $\ell \in [1:L]$ to index each RIS. Let N_ℓ be the number of REs in the ℓth RIS and $\boldsymbol{\theta}_\ell = [e^{j\theta_{\ell_1}}, e^{j\theta_{\ell_2}}, \ldots, e^{j\theta_{\ell_{N_\ell}}}]^\top$ be the reflection coefficients vector of the ℓth RIS, where θ_{ℓ_n} is the phase shift of the n_ℓth RE in the ℓth RIS. The reflective coefficients matrix at the ℓth RIS is denoted by $\boldsymbol{\Psi}_\ell = \mathrm{diag}(\boldsymbol{\theta}_\ell)$. From a practical stand [22], [32], [51]–[54], we also assume that each phase shift θ_{ℓ_n} is limited to a discrete set

$$\Phi_{K_\ell} = \{0, \ldots, k\omega, \ldots, (K_\ell - 1)\omega\} \quad \text{where } \omega = \frac{2\pi}{K_\ell}, \tag{1}$$

for some positive integer $K_\ell \geq 2$.

Both parallel and cascaded topologies of the multi-RIS design are considered in this work. In the parallel topology, each RIS independently reflects signals towards the BS without any RIS interacting with another. In the cascaded topology, in addition to the link between each RIS and the BS, the RISs are connected in series, and the signal reflected by one RIS is further reflected by subsequent RISs before reaching the BS. Due to the characteristics of indoor localization task, we adopt the line-of-sight (LoS) channel model in which the channels mainly depend on the geometric relationship between user, RISs and BS [14], [18], [33], [50]. Denote by $\boldsymbol{h}_\ell \in \mathbb{C}^{N_\ell}$ the reflective channel vector from the user to the ℓth RIS, and denote by $\boldsymbol{G}_\ell \in \mathbb{C}^{M \times N_\ell}$ the reflective channel matrix from the ℓth RIS to the BS. Let (ϕ_ℓ, ψ_ℓ) be the azimuth and elevation angle of AoD from the ℓth RIS to the user which are *unknown* for us. Therefore, the reflective channel vector $\boldsymbol{h}_\ell$ is given by

$$\boldsymbol{h}_\ell = \kappa_\ell \cdot \boldsymbol{a}^{\mathrm{RIS}}(\phi_\ell, \psi_\ell), \tag{2}$$

where κ_ℓ is the pathloss between the user and the ℓth RIS, $\boldsymbol{a}^{\mathrm{RIS}}$

TABLE I: List of Main Variables

Symbol	Definition
L	number of RISs
N_ℓ	number of REs of RIS ℓ
T	number of random samples for localization
n_ℓ	index of the nth RE of RIS ℓ
K_ℓ	number of phase shift choices for each RE of RIS ℓ
θ_{n_ℓ}	phase shift of RE n_ℓ
$\boldsymbol{\Psi}_\ell$	reflective coefficients matrix of RIS ℓ
$\boldsymbol{d}$	direct channel vector form the user to the BS
$\boldsymbol{G}_\ell$	reflective channel matrix from the RIS ℓ to the BS
$\boldsymbol{h}_\ell$	reflective channel vector from the user to the RIS ℓ
η_ℓ	azimuth from the RIS ℓ to the BS
ϑ_ℓ	elevation from the RIS ℓ to the BS
ϕ_ℓ	azimuth from the RIS ℓ to the user
ψ_ℓ	elevation from the RIS ℓ to the user
δ_ℓ	AoA from the RIS ℓ t o the BS
$\zeta_{\ell,u}$	azimuth from the RIS ℓ to the RIS u
$\iota_{\ell,u}$	elevation from the RIS ℓ to the RIS u
$\mu_{u,\ell}$	azimuth from the RIS u to the RIS ℓ
$\nu_{u,\ell}$	elevation from the RIS u to the RIS ℓ

denotes the steering vector, and its nth element is expressed as

$$[\boldsymbol{a}^{\text{RIS}}(\phi_\ell,\psi)]_{n_\ell} = e^{j\frac{2\pi r_{I_\ell}}{\lambda_c}\{v_1(n_\ell,C_\ell)\sin\phi_\ell\cos\psi_\ell + v_2(n_\ell,C_\ell)\sin\psi_\ell\}}, \tag{3}$$

where r_{I_ℓ} is the distance two adjacent REs of the ℓth RIS, λ_c is carrier wavelength, $v_1(n_\ell,C_\ell) = \text{mod}(n_\ell-1,C_\ell)$ and $v_2(n_\ell,C_\ell) = \lfloor\frac{n_\ell-1}{C_\ell}\rfloor$ with C_ℓ being the number of columns of the RIS. Let $(\eta_\ell,\vartheta_\ell)$ denotes the azimuth and elevation from the ℓth RIS to the BS which are already known at the BS. Let δ_ℓ be the AoA from the ℓth RIS to the BS which is also known. The channel matrix $\boldsymbol{G}_\ell$ can be written as

$$\boldsymbol{G}_\ell = \epsilon_\ell \cdot \boldsymbol{a}^{\text{BS}}(\delta_\ell)\boldsymbol{a}^{\text{RIS}}(\eta_\ell,\vartheta_\ell)^{\mathsf{H}}, \tag{4}$$

where ϵ_ℓ is the pathloss component, and the steering vector of the BS is given by

$$\boldsymbol{a}^{\text{BS}}(\delta_\ell) = \left[1,\ldots,e^{j\frac{2\pi(M-1)r_A}{\lambda_c}\cdot\cos\delta_\ell}\right]^\top, \tag{5}$$

where r_A is the distance two adjacent antennas of the BS. Denote by $\boldsymbol{H}_{\ell,u} \in \mathbb{C}^{N_\ell\times N_u}, \ell > u$ the cascaded channel matrix between the ℓth RIS and the uth RIS, which is given by

$$\boldsymbol{H}_{\ell,u} = \beta_{\ell,u}\cdot\boldsymbol{a}^{\text{RIS}}(\zeta_{\ell,u},\iota_{\ell,u})\boldsymbol{a}^{\text{RIS}}(\mu_{u,\ell},\nu_{u,\ell})^{\mathsf{H}}, \tag{6}$$

where $\beta_{\ell,u}$ is the pathloss component, $(\zeta_{\ell,u},\iota_{\ell,u})$ is AoD pair from RIS ℓ to RIS u and $(\mu_{u,\ell},\nu_{u,\ell})$ is AoD pair from RIS u to RIS ℓ. Moreover, the the direct channel from the user to the BS, denoted by $\boldsymbol{d}\in\mathbb{C}^M$, exists and is expressed in polar form as:

$$\boldsymbol{d} = \rho\cdot\left[e^{j\xi_1},\ldots,e^{j\xi_M}\right]^\top, \tag{7}$$

where ρ is the pathloss component of direct channel, $\{\xi_1,\ldots,\xi_M\}$ are the phase angles.

B. Signal Transmission and Reception

In order to effectively circumvents the limitations of existing RIS-assisted localization approaches as listed in Section I, we design a passive localization approach, based on the signal transmission and reception, which are detailed as follows. Specifically, we first generate a codebook that includes a total of T random RIS phase shift samples $\boldsymbol{\Theta}^{(t)}$, with the sample index $t\in[1:T]$, and each random sample contains L random subsets, i.e., $\boldsymbol{\Theta}^{(t)} = [\boldsymbol{\theta}_1^{(t)},\ldots,\boldsymbol{\theta}_L^{(t)}]$, with the subset index $\ell\in[1:L]$. With each $\theta_{n_\ell}^{(t)}$ uniformly drawn from Φ_{K_ℓ}, the ℓth random subset of tth sample is generated as

$$\boldsymbol{\theta}_\ell^{(t)} = \left\{e^{j\theta_{n_\ell}^{(t)}} \,\middle|\, n_\ell\in[1:N_\ell]\right\}. \tag{8}$$

The codebook is then shared between the BS and the RIS controller, and the RIS controller then allocates each random subset $\boldsymbol{\theta}_\ell^{(t)},\forall\ell$, to the corresponding RIS with the same index ℓ across T time slots, which is also shown in Fig. 1.

In each time slot t, the signal transmitted by the user is denoted by $s(t)$ with transmit power $|s^{(t)}|^2 = P$. It is important to note that the user transmits its originally intended message $s^{(t)}$, to the BS, rather than the pilot signal. In the following, we detail the signal reception at the BS for two distinct RIS topologies, namely, the parallel topology, where each RIS reflects signals independently, and the cascaded topology, where RISs reflect signals sequentially:

1) Parallel Topology Case: We start with the simpler case that the RISs are deployed in the parallel topology. In this case, only direct links exist between each RIS and the BS, and between the user and each RIS, with no interaction between the RISs. There are no cascaded channels among the RISs, and their effects on the system can be considered independently. Since the RISs do not interfere with each other, the overall channel can be treated as the linear sum of the individual single-hop channels between each RIS and the BS, and between the user and each RIS. The received signal at the BS is therefore given as

$$\boldsymbol{y}^{(t)} = \left(\boldsymbol{d} + \sum_{\ell=1}^{L}\boldsymbol{G}_\ell\boldsymbol{\Psi}_\ell\boldsymbol{h}_\ell\right)s^{(t)} + \boldsymbol{z}^{(t)}, \tag{9}$$

where $\boldsymbol{z}^{(t)}\in\mathbb{C}^M$ is the additive white Gaussian noise (AWGN) received at the BS. Recall that $\boldsymbol{d}$ represents the direct channel between the BS and the user as defined in (7). $\sum_{\ell=1}^{L}\boldsymbol{G}_\ell\boldsymbol{\Psi}_\ell\boldsymbol{h}_\ell$ denotes the effective channel encompassing the transmission from the user to L parallel RISs and subsequently to the BS. $\boldsymbol{G}_\ell$, $\boldsymbol{\Psi}_\ell$ and $\boldsymbol{h}_\ell$ are specified in (2)–(5).

In this case, the received signal at the mth antenna of the BS can be expressed as

$$[\boldsymbol{y}^{(t)}]_m = \left([\boldsymbol{d}]_m + \sum_{\ell=1}^{L}\sum_{n_\ell=1}^{N}Q_{m,n_\ell}e^{j\theta_{n_\ell}}\right)s^{(t)} + [\boldsymbol{z}^{(t)}]_m, \tag{10}$$

where $Q_{m,n_\ell} = [\boldsymbol{G}]_{m,n_\ell}\cdot[\boldsymbol{h}_\ell]_{n_\ell}$ represents the reflective channel from the user to the mth antenna at the BS, with the signal being reflected by the n_ℓth RE of the ℓth RIS.

Notably, the single RIS case can be treated as a special case of the parallel topology case. When $L=1$, we omit

the subscript ℓ for simplicity, the received signal at the BS $\boldsymbol{y}^{(t)} \in \mathbb{C}^M$ is

$$\boldsymbol{y}^{(t)} = \big(\boldsymbol{d} + \boldsymbol{G}\boldsymbol{\Psi}\boldsymbol{h}\big)s^{(t)} + \boldsymbol{z}^{(t)}. \tag{11}$$

The received signal at the mth antenna of the BS can be further expressed as

$$[\boldsymbol{y}^{(t)}]_m = \left([\boldsymbol{d}]_m + \sum_{n=1}^{N} Q_{m,n} e^{j\theta_n}\right)s^{(t)} + [\boldsymbol{z}^{(t)}]_m, \tag{12}$$

where $Q_{m,n} = [\boldsymbol{G}]_{m,n} \cdot [\boldsymbol{h}]_n$ represents the reflective channel from the user to the mth antenna at the BS, with the signal being reflected by the nth RE of the RIS. Thus, we first consider this special case and further extend it to the multiple RIS case.

2) Cascaded Topology Case: We then consider the general case, where there are no preliminary requirements on the placement of multiple RISs and the cascaded channel among the RISs exists. The received signal vector at the BS is then given by

$$\begin{aligned}\boldsymbol{y}^{(t)} =& \Bigg(\boldsymbol{d} + \sum_{\ell=1}^{L} \boldsymbol{G}_\ell \boldsymbol{\Psi}_\ell \boldsymbol{h}_\ell \\ &+ \sum_{\ell=1}^{L}\sum_{v=\ell+1}^{L} \boldsymbol{G}_\ell \boldsymbol{\Psi}_\ell \Big(\prod_{u=\ell+1}^{v} \boldsymbol{H}_{u-1,u}\boldsymbol{\Psi}_u\Big)\boldsymbol{h}_v\Bigg)s^{(t)} + \boldsymbol{z}^{(t)},\end{aligned} \tag{13}$$

where $\boldsymbol{z}^{(t)} \sim \mathcal{CN}(0, \sigma^2 \boldsymbol{I}_M)$ is the background noise.

In this case, the received signal at the mth antenna of the BS can be written as

$$\begin{aligned}[\boldsymbol{y}^{(t)}]_m =& \Big([\boldsymbol{d}]_m + \sum_{n_\ell \in [0:N]^L, \forall \ell} Q_{m,n_1,\ldots,n_L} e^{j\sum_{\ell=1}^{L}\theta_{n_\ell}}\Big)s^{(t)} \\ &+ [\boldsymbol{z}^{(t)}]_m,\end{aligned} \tag{14}$$

where $Q_{m,n_1,\ldots,n_L}$ represents the cascaded reflective channel from the user to the mth antenna at the BS, with the signal being reflected by the n_1th RE of the 1st RIS, the n_2th RE of the 2nd RIS, until the n_Lth RE of the Lth RIS. from the user to the mth antenna.

The BS measures and records the received signal power at each antenna over T time slots. In each time slot t, the received signal power measurement $\left|[\boldsymbol{y}^{(t)}]_m\right|^2, \forall m$ corresponds to the tth random sample $\boldsymbol{\Theta}^{(t)}$. Based on these measurements, the proposed RAPL method proceeds to achieve passive localization, as detailed in the following sections. It is worth noting that the above signal transmission and reception do not require pilot signals and CSI, the communication process therefore remains uninterrupted. In addition, the BS and the RIS controller only share the codebook and perform synchronization, with no additional interactions required. Moreover, the proposed RAPL does not require extensive offline data training beforehand. Instead, it only needs to allocate random phase shifts and collect received power measurements online when a localization task arises.

C. Problem Statement

Recall that we aim to estimate the *unknown* user position $\boldsymbol{p}$ based on the received signal strength measurements across T time slots, without any channel information. As previously stated, the proposed RAPL is divided into two stages: (i) AoD pairs estimation which contains phase shift difference estimation and recovering the AoD pairs, and (ii) pinpointing the position of the user. The specific problems addressed in each stage are detailed as follows:

1) AoD Pairs Estimation: We start by formulating the problem of AoD pairs estimation in the first stage. Denote by $\hat{\boldsymbol{\chi}}_\ell = (\hat{\phi}_\ell, \hat{\psi}_\ell)$ the estimation of the ℓth AoD pair which indicates the direction from the ℓth RIS to the user, where $\hat{\phi}_\ell$ is the azimuth estimation and $\hat{\psi}_\ell$ is the elevation estimation. The goal of this stage is to obtain $\hat{\boldsymbol{\chi}}_\ell$ based on the received signal power $\left|[\boldsymbol{y}^{(t)}]_m\right|^2, \forall m, t$. Specifically, after obtaining all received signal power measurements, the ℓth estimated AoD pair is produced as a function:

$$\hat{\boldsymbol{\chi}}_\ell = \mathcal{F}\Big(\left|[\boldsymbol{y}^{(t)}]_m\right|^2\Big),\ \forall m, t, \tag{15}$$

where $\mathcal{F}(\cdot)$ denotes the ℓth AoD pair estimation approach that the mapping from all received signal power measurements to each estimated AoD pair. Thus, the AoD pair estimation problem which is consistent with the problem formulations in [33], [50] can be expressed as:

$$\underset{\mathcal{F}(\cdot)}{\text{minimize}} \quad \|\boldsymbol{\chi}_\ell - \hat{\boldsymbol{\chi}}_\ell\|_2^2,\ \forall \ell \tag{16a}$$

$$\text{subject to} \quad \theta_{n_\ell} \in \Phi_K,\ \forall n_\ell, \tag{16b}$$

$$\hat{\boldsymbol{\chi}}_\ell = \mathcal{F}\Big(\left|[\boldsymbol{y}^{(t)}]_m\right|^2\Big),\ \forall m, t, \ell. \tag{16c}$$

The phase shift $\theta_{n_\ell}, \forall n_\ell$ can be only chosen from the discrete set specified in (16b). In Section III, we provide a detailed explanation of the proposed PARL approach for solving (16) in a single RIS scenario.

2) Pinpointing the User Position: In the single-RIS scenario, only the direction from the user to the RIS can be determined. However, in the multi-RIS case, by leveraging the estimated AoD pairs from multiple RISs, the user's position can be accurately pinpointed. Here, we formulate the problem in the second stage for pinpointing the position of the user from the AoD pairs. Denote by $\hat{\boldsymbol{p}}$ the estimated user position, the function that producing $\hat{\boldsymbol{p}}$ is given by

$$\hat{\boldsymbol{p}} = \mathcal{L}(\boldsymbol{\chi}_\ell), \forall \ell, \tag{17}$$

where $\mathcal{L}(\cdot)$ denotes the localization approach that pinpointing the user position based on the estimated AoD pairs. The localization problem of the second stage is formulated as:

$$\underset{\mathcal{L}(\cdot)}{\text{minimize}} \quad \|\boldsymbol{p} - \hat{\boldsymbol{p}}\|_2^2 \tag{18a}$$

$$\text{subject to} \quad \hat{\boldsymbol{p}} = \mathcal{L}(\hat{\boldsymbol{\chi}}_\ell), \forall \ell. \tag{18b}$$

The proposed localization approach $\mathcal{L}(\cdot)$ is detailed in Section IV for both parallel and cascaded topology RIS cases.

III. Direction Estimation with Single RIS

In this section, we propose a novel AoD pairs estimation approach to address (16) for the first stage. Since the estimation of AoD pairs in the case with multiple RISs is a simple extension of the single RIS case, we start with the single RIS

case, i.e., $L = 1$. Also we omit the subscript ℓ for simplicity. Specifically, we estimate the direction from the RIS to the user by directly deriving the AoD pair $\hat{\boldsymbol{\chi}}$ from the statistical information extracted from received signal power samples and the corresponding codebook of the RIS phase shift vectors.

A. Phase Shift Difference Estimation

We begin with reiterating that $[\boldsymbol{d}]_m$ represents the direct channel between the user and the mth antenna of the BS, and $Q_{m,n}$ denotes the reflective channel from the user to the mth antenna at the BS, with the signal being reflected by the nth RE of the RIS. Then, we start by defining the phase difference between $[\boldsymbol{d}]_m$ and $Q_{m,n}$, i.e.,

$$\Delta_{m,n} = \angle[\boldsymbol{d}]_m - \angle Q_{m,n}. \tag{19}$$

With each reflective coefficient θ_n uniformly and independently drawn in Φ_K, the expectation of the received signal power at the mth antenna of the BS is given by

$$\mathbb{E}\Big[\big|[\boldsymbol{y}]_m\big|^2\Big] = \rho^2 P + \sum_{\ell=1}^{N} \kappa^2\epsilon^2 P + \sigma^2. \tag{20}$$

Moreover, the expectation conditioned on $\theta_n = k\omega$ can be expressed as

$$\begin{aligned}\mathbb{E}\Big[\big|[\boldsymbol{y}]_m\big|^2\Big|\theta_n = k\omega\Big] = \rho^2 P + \sum_{q=1,q\neq n}^{N} \kappa^2\epsilon^2 P \\ + 2\kappa\epsilon P\cos(k\omega - \Delta_{m,n}) + \sigma^2.\end{aligned} \tag{21}$$

With the phase difference $\Delta_{m,n}$ defined in (19), we can write the difference between the two expectations, i.e.,

$$\begin{aligned}J_{m,n,k}(\Delta_{m,n}) &= \mathbb{E}\Big[\big|[\boldsymbol{y}]_m\big|^2\Big|\theta_n = k\omega\Big] - \mathbb{E}\Big[\big|[\boldsymbol{y}]_m\big|^2\Big] \\ &= 2\kappa\epsilon P\cos(k\omega - \Delta_{m,n}).\end{aligned} \tag{22}$$

Let $\mathcal{E}_{n,k} \subseteq [1:T]$ be the set of indices of those samples $\boldsymbol{\theta}^{(t)}$ satisfying $\theta_n^{(t)} = k\omega$, i.e.,

$$\mathcal{E}_{n,k} \triangleq \Big\{t \in [1:T]\Big|\theta_n^{(t)} = k\omega\Big\}. \tag{23}$$

Then, a conditional sample mean of $\big|[\boldsymbol{y}^{(t)}]_m\big|^2$ is computed for each $\mathcal{E}_{n,k}$ as

$$\widehat{\mathbb{E}}\left[|Y|^2|\theta_n = k\omega\right] \triangleq \frac{1}{|\mathcal{E}_{n,k}|}\sum_{t\in\mathcal{E}_{n,k}}\big|[\boldsymbol{y}^{(t)}]_m\big|^2. \tag{24}$$

Thus, we can evaluate each $J_{m,n,k}(\Delta_{m,n})$ empirically as $\hat{J}_{m,n,k}$ based on the random samples, i.e.,

$$\widehat{J}_{m,n,k} = \frac{1}{|\mathcal{E}_{n,k}|}\sum_{t\in\mathcal{E}_{n,k}}\big|[\boldsymbol{y}^{(t)}]_m\big|^2 - \frac{1}{T}\sum_{t=1}^{T}\big|[\boldsymbol{y}^{(t)}]_m\big|^2. \tag{25}$$

Denote by $\widehat{\Delta}_{m,n}$ the estimation of phase shift difference $\Delta_{m,n}$. We aim to find the optimal phase shift difference estimation based on the above theoretical expectations and calculated sample means.

Theorem 1: Based on (22) *and* (25)*, the optimal estimation* $\widehat{\Delta}^{\star}_{m,n}$ *is given by*

$$\widehat{\Delta}^{\star}_{m,n} = \arctan\frac{\sum_{k=1}^{K}\widehat{J}_{m,n,k}\sin k\omega}{\sum_{k=1}^{K}\widehat{J}_{m,n,k}\cos k\omega}. \tag{26}$$

Proof: We can estimate $\Delta_{m,n}$ by minimizing the gap between $J_{m,n,k}$ and $\widehat{J}_{m,n,k}$. In particular, with the *sum-of-squares* metric, i.e.,

$$\delta_{m,n}(\Delta_{m,n}) = \sum_{k=1}^{K}\Big|J_{m,n,k}(\Delta_{m,n}) - \widehat{J}_{m,n,k}\Big|^2, \tag{27}$$

the distortion minimizing problem is given as

$$\underset{\Delta_{m,1},\ldots,\Delta_{m,N}}{\text{minimize}} \quad \delta_{m,n}(\Delta_{m,n}) \tag{28a}$$

$$\text{subject to} \quad 0 \le \Delta_{m,n} \le 2\pi, \text{for all } n = 1,\ldots,N. \tag{28b}$$

This problem is convex and can be solved by

$$\begin{aligned}&\frac{\partial\delta_{m,n}(\Delta_{m,n})}{\partial\Delta_{m,n}} \\ =&4\sum_{k=1}^{K}\kappa^2\epsilon^2P^2\sin(k\omega - \Delta_{m,n})\cos(k\omega - \Delta_{m,n}) \\ &- 4\kappa\epsilon P\cdot\widehat{J}_{m,n,k}\cdot\sin(k\omega - \Delta_{m,n}) \\ =&0.\end{aligned} \tag{29}$$

Then, we obtain

$$\sum_{k=1}^{K}\widehat{J}_{m,n,k}\cdot\sin(k\omega - \Delta_{m,n}) = 0. \tag{30}$$

Expanding (30), we obtain

$$\cos\Delta_{m,n}\cdot\sum_{k=1}^{K}\widehat{J}_{m,n,k}\sin k\omega = \sin\Delta_{m,n}\cdot\sum_{k=1}^{K}\widehat{J}_{m,n,k}\cos k\omega. \tag{31}$$

Thus, the optimal estimation of phase difference can be finally obtained by

$$\widehat{\Delta}^{\star}_{m,n} = \arctan\frac{\sum_{k=1}^{K}\widehat{J}_{m,n,k}\sin k\omega}{\sum_{k=1}^{K}\widehat{J}_{m,n,k}\cos k\omega}. \tag{32}$$

■

B. Recovering the AoD Pair

After obtaining the optimal estimation $\widehat{\Delta}_{m,n}$, we can further recover $\hat{\psi}$ and $\hat{\phi}$ by utilizing the phase relationship between the reflective channels induced by two adjacent REs in the LoS channel model.

Specifically, as defined in (19), the phase difference between the direct channel and the ith reflective channel from the user to the mth antenna of BS is given by

$$\begin{aligned}\Delta_{m,i} =&\zeta_m - \frac{2\pi r_I}{\lambda_c}\Big(v_1(i,C)\sin\phi\cos\psi + v_2(i,C)\sin\psi \\ &- v_1(i,C)\sin\eta\cos\vartheta - v_2(i,C)\sin\vartheta\Big), \\ &i = 1,\ldots,N-C,\end{aligned} \tag{33}$$

$$\Delta_{m,i+C} = \zeta_m - \frac{2\pi r_I}{\lambda_c}\Big(v_1(i+C,C)\sin\phi\cos\psi + v_2(i+C,C)\sin\psi - v_1(i+C,C)\sin\eta\cos\vartheta - v_2(i+C,C)\sin\vartheta\Big), \quad i = 1,\ldots,N-C. \tag{35}$$

$$\begin{aligned}\Delta_{m,i} - \Delta_{m,i+C} =& \frac{2\pi r_I}{\lambda_c}\Big(-v_1(i,C)\sin\phi\cos\psi - v_2(i,C)\sin\psi + v_1(i,C)\sin\eta\cos\vartheta + v_2(i,C)\sin\vartheta\Big) \\ &+ \frac{2\pi r_I}{\lambda_c}\Big(v_1(i+C,C)\sin\phi\cos\psi + v_2(i+C,C)\sin\psi - v_1(i+C,C)\sin\eta\cos\vartheta - v_2(i+C,C)\sin\vartheta\Big) \\ =& \frac{2\pi r_I}{\lambda_c}(\sin\psi - \sin\vartheta), \quad i = 1,\ldots,N-C.\end{aligned} \tag{36}$$

where

$$\zeta_m = \xi_m - \frac{2\pi(m-1)r_A}{\lambda_c}\cos\delta. \tag{34}$$

The phase difference between the direct channel from the user to the mth antenna at the BS and the reflective channel from the user to the same antenna, assisted by the $(i+C)$th RE (the adjacent RE in the same column as the ith RE), is given by (35) at the top of the next page. The gap between $\Delta_{m,i}$ and $\Delta_{m,i+C}$ can be further computed by (36) at the top of the next page. Therefore, the estimated elevation angle between the RIS and the user $\hat{\psi}_{m,i}$ can be recovered by

$$\hat{\psi}_{m,i} = \arcsin\Big\{\frac{\lambda_c(\hat{\Delta}_{m,i} - \hat{\Delta}_{m,i+C})}{2\pi r_I} + \sin\vartheta\Big\}. \tag{37}$$

We estimate $\hat{\psi}_{m,i}$ for each antenna of the BS in a sequential fashion. A total of $M(N-C)$ estimated elevations will be finally obtained. By taking the arithmetic mean of all $M(N-C)$ estimated elevation values, we obtain the final estimated elevation angle $\hat{\psi}$, i.e.,

$$\hat{\psi} = \frac{\sum_{m=1}^{M}\sum_{i=1}^{N-C}\hat{\psi}_{m,i}}{M(N-C)}. \tag{38}$$

By following the same derivation procedure, we can subsequently obtain the estimated azimuth. Specifically, we also express the phase difference between the direct channel and the jth reflective channel from the user to the mth antenna of BS as

$$\begin{aligned}\Delta_{m,j} =& \zeta_m - \frac{2\pi r_I}{\lambda_c}\Big(v_1(j,C)\sin\phi\cos\psi + v_2(j,C)\sin\psi \\ &- v_1(j,C)\sin\eta\cos\vartheta - v_2(j,C)\sin\vartheta\Big), \\ & j \neq J,\end{aligned} \tag{39}$$

where $J = \Big(\lfloor\frac{j-1}{C}\rfloor + 1\Big)\times C$, and the phase difference between the direct channel from the user to the mth antenna at the BS and the reflective channel from the user to the same antenna, assisted by the $(j+1)$th RE (the adjacent RE in the same row as the jth RE) is given by (42) at the top of next page. The gap between the $\Delta_{m,j}$ and $\Delta_{m,j+1}$ can be further computed by (43) at the top of next page. Hence, the estimated azimuth angle between the RIS and the user $\hat{\phi}_{m,j}$ can be recovered by

$$\hat{\phi}_{m,j} = \arcsin\Big\{\frac{\lambda_c(\widehat{\Delta}_{m,j} - \widehat{\Delta}_{m,j+1})}{2\pi r_I\cos\hat{\psi}} + \frac{\sin\eta\cos\vartheta}{\cos\hat{\psi}}\Big\}. \tag{40}$$

Algorithm 1 RAPL–AoD Pair Estimation Algorithm

```
Generate T random samples for each RIS.
for t = 1, ..., T do
    Measure the received signal power |[y^(t)]_m|^2, ∀m.
end for
for m = 1, ..., M do
    for n = 1, ..., N do
        for k = 1, ..., K do
            Compute Ĵ_{m,n,k} in (25).
        end for
        Compute Δ̂_{m,n} in (32).
    end for
end for
for m = 1, ..., M do
    for i = 1, ..., N − C do
        Compute Δ̂_{m,i} − Δ̂_{m,i+C}.
        Compute ψ̂_{m,i} in (37).
    end for
end for
Obtain the estimated elevation ψ̂ by (38)
for m = 1, ..., M do
    for j = 1, ..., N.  j ≠ J do
        Compute Δ̂_{m,j} − Δ̂_{m,j+1}.
        Compute φ̂_{m,j} in (40).
    end for
end for
Obtain the estimated azimuth φ̂ by (41)
Output: χ̂ = (φ̂, ψ̂).
```

We also take the arithmetic mean of a total of $M \times \frac{N(C-1)}{C}$ estimated azimuth values, then we obtain the final estimated azimuth $\hat{\phi}$, i.e.,

$$\hat{\phi} = \frac{C\times\sum_{m=1}^{M}\sum_{\substack{j=1,\\ j\neq J}}^{N-1}\hat{\phi}_{m,j}}{MN(C-1)}. \tag{41}$$

The above AoD pair estimation method $\mathcal{F}(\cdot)$ is summarized in Algorithm 1. For a L-RIS system, i.e., $L \geq 2$, we can simply extend the proposed AoD pair estimation approach that estimating each AoD pair $\hat{\boldsymbol{\chi}}_\ell = (\hat{\phi}_\ell, \hat{\psi}_\ell), \forall \ell$ in a sequential fashion which is introduced in the next Section. After obtaining all AoD pairs, we can further pinpoint the potential position area of the user based on these AoD pairs, which will be also shown in the next section.

$$\Delta_{m,j+1} = \zeta_m - \frac{2\pi r_I}{\lambda_c}\Big(v_1(j+1,C)\sin\phi\cos\psi + v_2(j+1,C)\sin\psi - v_1(j+1,C)\sin\eta\cos\vartheta - v_2(j+1,C)\sin\vartheta\Big), \quad j \neq J. \tag{42}$$

$$\begin{aligned}\Delta_{m,j} - \Delta_{m,j+1} =& \frac{2\pi r_I}{\lambda_c}\Big(-v_1(j,C)\sin\phi\cos\psi - v_2(j,C)\sin\psi + v_1(j,C)\sin\eta\cos\vartheta + v_2(j,C)\sin\vartheta\Big) \\ &+ \frac{2\pi r_I}{\lambda_c}\Big(v_1(j+1,C)\sin\phi\cos\psi + v_2(j+1,C)\sin\psi - v_1(j+1,C)\sin\eta\cos -\vartheta v_2(j+1,C)\sin\vartheta\Big) \\ =& \frac{2\pi r_I}{\lambda_c}(\sin\phi\cos\psi - \sin\eta\cos\vartheta), \quad j \neq J.\end{aligned} \tag{43}$$

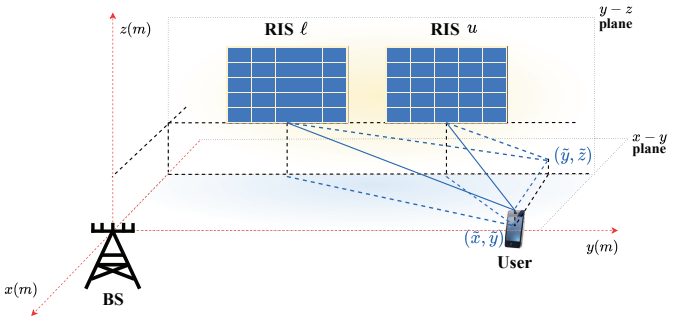

Fig. 2: Projections of rays originating from RISℓ and RISu onto the x-y and y-z planes.

IV. Localization with Multiple RISs

As mentioned in the end of Section III, the proposed AoD pair estimation approach $\mathcal{F}(\cdot)$ indeed could be further extended to the multiple RISs cases, i.e., $L \geq 2$. We then propose an approach $\mathcal{L}(\cdot)$ for the second stage that pinpointing the user position in multiple RISs network based on the AoD pair estimations. In the following section, we elaborate on the approaches in two cases: i) parallel topology case, and ii) cascaded topology case. Additionally, the summary of the proposed approach, complexity analysis and the advantages of the proposed approach are presented in Section IV-C.

A. Parallel Topology Case

Same as the single-RIS case, we first generate a codebook which consists T random samples, for the sample index $t \in [1:T]$. The BS then also measure the received signal power at each antenna for all time slot t, i.e., $\left|[\boldsymbol{y}^{(t)}]_m\right|^2, \forall m$.

As mentioned in Section II, only the single-hop channels are considered in the parallel topology. Since there is no cascaded channel, the estimation process for the AoD pair corresponding to each RIS is independent. Therefore, we can perform L independent calculations according to Algorithm 1 to estimate the L AoD pairs $\hat{\boldsymbol{\chi}}_\ell = (\hat{\phi}_\ell, \hat{\psi}_\ell), \forall \ell$, with each random samples $\boldsymbol{\theta}_\ell^{(t)} = \{e^{j\theta_{n_\ell}^{(t)}} | n_\ell \in [1:N_\ell]\}, \forall \ell$ and corresponding received signal power $\left|[\boldsymbol{y}^{(t)}]_m\right|^2, \forall m$.

For any given AoD pair $\boldsymbol{\chi}_\ell = (\phi_\ell, \psi_\ell)$, we can obtain a ray in three-dimensional space originating from the position of the ℓth RIS. For any two given AoD pairs, we can determine two rays in space. The projections of these rays on the x-y and y-z planes will intersect, which is shown in Fig. 2, allowing us to estimate the user's location based on the intersection points.

Algorithm 2 RAPL–Pinpointing the User Position Algorithm

1: **input:** $\hat{\boldsymbol{\chi}}_\ell, \forall \ell$.
2: **for** $\ell = 1, 2, \ldots, L$ **do**
3: Compute $(\tilde{x}_\ell, \tilde{y}_\ell, \tilde{z}_\ell)$ in (44), (45) and (46).
4: **end for**
5: Compute $\hat{\boldsymbol{p}}$ in (47).
6: **Output:** $\hat{\boldsymbol{p}}$.

It is important to note that we typically assume all RISs are deployed on the same y-z plane, so the projections of the two rays on the x-z plane may not intersect. Therefore, we do not consider the projections on the x-z plane.

As mentioned earlier, the positions of the RISs are known, i.e., the three-dimensional coordinates for the RISs $(x_\ell, y_\ell, z_\ell), \ell = 1, \ldots, L$ are known. Also we have obtained the estimated ℓth AoD pair $\hat{\boldsymbol{\chi}}_\ell = (\hat{\phi}_\ell, \hat{\psi}_\ell)$ and uth AoD pair $\hat{\boldsymbol{\chi}}_u = (\hat{\phi}_u, \hat{\psi}_u)$ by Algorithm 1. We can obtain the intersection point $(\tilde{x}, \tilde{y})$ of the projections of the two rays originating from the ℓth RIS and the uth RIS on the x-y plane can be expressed as

$$\tilde{x} = \frac{(y_u - x_u\cot\hat{\phi}_u) - (y_\ell - x_\ell\cot\hat{\phi}_\ell)}{\cot\hat{\phi}_\ell - \cot\hat{\phi}_u}, \tag{44}$$

$$\tilde{y} = \tilde{x}\cot\hat{\phi}_\ell + (y_\ell - x_\ell\cot\hat{\phi}_\ell). \tag{45}$$

Then we further confirm the $\tilde{z}$ by

$$\tilde{z} = \frac{1}{2}\left[(z_\ell + z_u) - \tilde{y}\left(\frac{1}{\tan\hat{\psi}_\ell\cos\hat{\phi}_\ell} + \frac{1}{\tan\hat{\psi}_u\cos\hat{\phi}_u}\right)\right]. \tag{46}$$

Therefore, based on the aforementioned procedure, the estimation of the user position $\tilde{\boldsymbol{p}} = (\tilde{x}, \tilde{y}, \tilde{z})$ is obtained.

For a L-RIS network, there are a total of $\varrho = \frac{L\times(L-1)}{2}$ possible combinations of AoD pairs. Therefore, we can obtain $\frac{L\times(L-1)}{2}$ estimated positions. The final estimation of the user's position is the average of all estimations, i.e.,

$$\hat{\boldsymbol{p}} = \frac{2\times\sum_{\varrho=1}^{\frac{L\times(L-1)}{2}}\tilde{\boldsymbol{p}}_\varrho}{L\times(L-1)} \tag{47}$$

The overall approach that pinpointing the user position $\mathcal{L}(\cdot)$ is summarized in Algorithm 2. It's important to emphasize that the proposed localization approach requires $L \geq 2$. The estimation performance improves as the number of RISs

$$[\boldsymbol{y}^{(t)}]_m = \Bigg(\underbrace{\underbrace{[\boldsymbol{d}]_m}_{\text{direct channel}} + \underbrace{\sum_{\substack{(n_1,\ldots,n_b,\ldots,n_L)\in[0:N]^{L-1} \\ b\neq\ell}} B_{m,n_1,\ldots,n_b,\ldots,n_L} e^{j\sum_{b=1,b\neq\ell}^{L}\theta_{n_b}}}_{\text{reflected channels due the fixed RISs}} + \underbrace{\sum_{n_\ell=1}^{N} W_{m,n_\ell} e^{j\theta_{n_\ell}}}_{\text{reflected channels due to RIS } \ell} }_{\text{equivalent direct channel}} \Bigg) \boldsymbol{s}^{(t)} + [\boldsymbol{z}^{(t)}]_m, \tag{48}$$

increases.

B. Cascaded Topogoly Case

When considering the case with cascaded channels, the approach of phase difference estimation (32) is not applicable, and recovering AoD pairs $(\hat{\phi}_\ell, \hat{\psi}_\ell)$ becomes much difficult. Here, we proposed a heuristic localization approach that estimating the phase difference and recovering each AoD pair in a sequential fashion.

Inspired by [32], we apply the above AoD pair estimation approach $\mathcal{F}(\cdot)$ sequentially for each RIS, estimating the AoD pair $(\hat{\phi}_\ell, \hat{\psi}_\ell)$ for the user with respect to each RIS ℓ one by one. Specifically, when configuring random phase shifts for a specific RIS based on the approach specified in Algorithm 1, the phase shifts of other RISs remain fixed. At the mth antenna of the BS, the received signal (14) can be rewritten as (48), where W_{m,n_ℓ} is reflected channel assisted by the n_ℓth RE of the ℓth RIS and this RIS is assumed to be configured with random phase shifts, $B_{m,n_1,\ldots,n_b,\ldots,n_L}, b \neq \ell$ represents the channel assisted by the n_bth RE of the RIS b with fixed phase shifts.The direct channel and the fixed reflected channels can be treated as an effective direct channel, denoted as V_m. Thus, (48) can be further written as

$$[\boldsymbol{y}^{(t)}]_m = \Big(V_m + \sum_{n_\ell=1}^{N} W_{m,n_\ell} e^{j\theta_{n_\ell}}\Big) s^{(t)} + [\boldsymbol{z}^{(t)}]_m. \tag{49}$$

After rewriting the signal model, we can extend our phase difference estimation method specified in Section III-A to this case. Specifically, $\widehat{\Delta}_{m,n_\ell} = \angle V_m - \angle W_{m,n_\ell}$ can be obtained by (32). Since the positions and angle information of BS and RISs are known, we can further recover the AoD pairs $(\hat{\phi}_\ell, \hat{\psi}_\ell)$ for all RISs, i.e., $\ell = 1, \ldots, L$.

With the sequential estimation, we finally obtain a total of $\frac{L\times(L-1)}{2}$ possible combinations of AoD pairs, and we can further pinpoint the location of the user by (44)–(47).

C. Summary of Proposed RAPL

After elaborating on the two stages that AoD pairs estimation and pinpointing the user position, we now summarize the proposed RAPL, the complexity, and summarize the advantages of proposed localization approach.

1) Summary of proposed RAPL: Recall that a codebook consists of T random samples, which is generated and shared between the BS and the RIS controller. The RIS controller then allocates the samples to each RIS across T time slots, which is specified in Section II-B. Moreover, in each time slot t, the BS is responsible for measuring and recording the received signal power at each antenna $\left|[\boldsymbol{y}^{(t)}]_m\right|^2, \forall m$ correspond to the tth random sample of the codebook. After obtaining the received signal power measurements, the user position can be confirmed in the two stages:

(i) AoD Pairs Estimation: Each AoD pair is estimated in a sequential fashion. For the ℓth AoD pair $\hat{\boldsymbol{\chi}}_\ell, \forall \ell$, we first estimate the phase difference $\widehat{\Delta}_{m,n}, \forall m, n$ between the direct channel and each reflective channel based on the conditional sample mean, the AoD pair is then recovered from the estimated phase difference based on the LoS channel model.

(ii) Pinpointing the User Position: With the L estimated AoD pairs, we finally pinpoint the user position based on the intersecting projections of rays originating from each RIS, the directions of which are determined by the AoD pairs.

2) Complexity: Then, we analyze the complexity of the proposed RAPL. For each RIS and each antenna at the BS, it requires $\mathcal{O}(\sum_\ell N_\ell T)$ to compute all the conditional sample mean values in received signal power, and it further requires $\mathcal{O}(\sum_\ell N_\ell K_\ell)$ to recover the AoD pair. For a total of L RISs and M received antennas at the BS, the computational complexity of AoD pairs estimation equals $\mathcal{O}(\sum_\ell MLN_\ell(K_\ell + T))$. The complexity of pinpointing the user position is $\mathcal{O}(L^2)$. Thus, the overall complexity of proposed RAPL is $\mathcal{O}(\sum_\ell MLN_\ell(K_\ell + T) + L^2)$.

3) Advantages: Compared to the limitations of the existing localization methods introduced in Section I, the advantages of the proposed RAPL are summarized as follows:

- ***No Need for CSI Acquisition*:** The proposed RAPL only need the recorded signal power measurements in the BS and the corresponding codebook, and the CSI is not required. Thus, the CSI acquisition can be eliminated. The conventional MMSE and MUSIC-based methods need the prior channel knowledge, which leads to significant additional overhead and compatibility issues with current 5G protocols.
- ***Without Communication Interruptions*:** In the signal transmission, the user still transmits its intended message to the BS in each time slot, the original communication is not interrupted. Most of pilots-assisted localization approaches need the communication interruptions for pilots transmission and reception.
- ***Limited Interactions between the RISs and the BS*:** The BS and RIS controller only share the codebook and synchronize with each other, without requiring a strong interaction. Some channel estimation-based methods and learning-based methods require that the codebook is

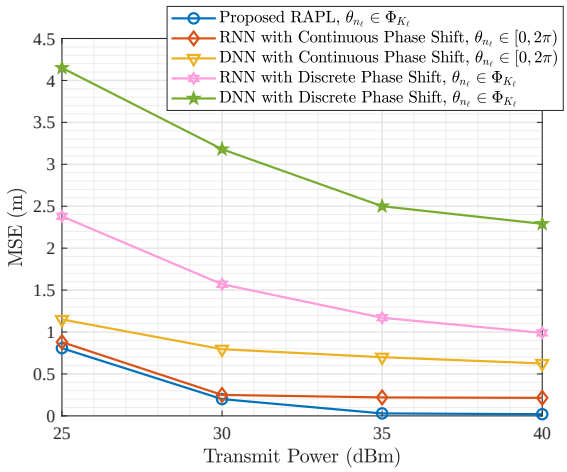

Fig. 3: Localization accuracy vs. transmit power in double-RIS MISO network with $N = 64$, $M = 8$.

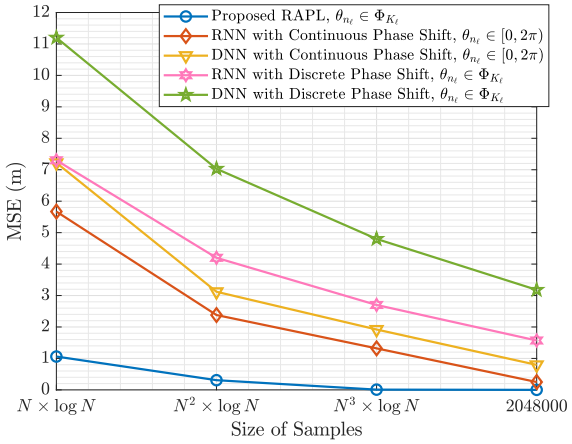

Fig. 4: Localization accuracy vs. size of training samples in double-RIS MISO network with $N = 64$, $M = 8$.

shared in real-time between the BS and the RISs. This necessitates strong interaction between the BS and RISs.

- ***Small Amounts of Training Data*:** The RAPL only needs to allocate random phase shifts and collect received power measurements online when a localization task arises. The size of random phase shift samples is much lower than the training data of learning-based methods. Indeed, acquiring great amounts of training data is challenging in practical networks.

The proposed RAPL can eliminate the limitations of existing methods as listed in Section I. Therefore, it is more practical and convenient to be deployed in the future industrial IoT and different edge networks.

V. Numerical Results

In this section, we evaluate the simulation results of the proposed RAPL. The simulation setting will be introduced in Section V-A, and the simulation results will be shown in Section V-B.

A. Simulation Setting

The channels are generated as follows: the LoS channel model is specified in Section II, and the pathloss models of the direct and reflected paths are $32.6 + 36.7\log(r_1)$ and $30 + 22\log(r_2)$, respectively, where r_1 and r_2 denote the corresponding link distance. We assume that $2\pi r_{I_\ell}/\lambda_c = 1, \forall \ell$, without loss of generality. The bandwidth is 10 MHz with a background noise of -170 dBm/Hz. The BS and the user are located at $(0m, 0m, 0m)$ and $(10m, 65m, -10m)$, respectively. The first RIS and the Lth RIS are located at $(-40m, 20m, 0m)$ and $(-40m, 60m, 0m)$. The remaining RISs are evenly distributed between the first and the Lth RIS, for instance, the location of ℓth RIS is $(-40m, 20 + (\ell - 1)\frac{40}{L}m, 0m), L > \ell > 1$. Assume that the BS also has 8 antennas and the uplink transmit power is 30 dBm.

Recall that ϕ_ℓ and ψ_ℓ denote the azimuth and the elevation AoDs from the ℓth RIS to the user. As shown in Fig. 1, the following mapping from the AoD pair $\boldsymbol{\chi}_\ell = \{\phi_\ell, \psi_\ell\}$ to the location of the user can be established:

$$\cos\phi_\ell \sin\psi_\ell = \frac{y - y_\ell^{\text{RIS}}}{r_\ell^{\text{RU}}}, \tag{50a}$$

$$\cos\psi_\ell = \frac{z_\ell^{\text{RIS}} - z}{r_\ell^{\text{RU}}}, \tag{50b}$$

where r_ℓ^{IU} denotes the distance between the ℓth RIS and the user. Recall that η_ℓ and ϑ_ℓ denote the azimuth and the elevation AoDs from the ℓth RIS to the BS. The following mapping form the AoD pair to the location of the user can be also established:

$$\cos\eta_\ell \sin\vartheta_\ell = \frac{y^{\text{BS}} - y_\ell^{\text{RIS}}}{r_\ell^{\text{BR}}}, \tag{51a}$$

$$\cos\vartheta_\ell = \frac{z_\ell^{\text{RIS}} - z^{\text{BS}}}{r_\ell^{\text{BR}}}, \tag{51b}$$

$$\sin\delta_\ell = \cos\vartheta_\ell, \tag{51c}$$

where r_ℓ^{BR} denotes the distance between the BS and the ℓth RIS. We assume that all RISs have the same number of REs, i.e., $N_1 = \cdots = N_L$, and that all K_ℓ values are fixed at 4 throughout the simulation tests, i.e., $\Phi_{K_\ell} = \{0, \frac{\pi}{2}, \pi, \frac{3\pi}{2}\}$ for all $\ell \in [1 : L]$.

When $L = 2$, the following methods are compared in our simulations:

- ***RNN-based method*:** This is a RNN-based active sensing method proposed in [33]. Note that this approach only considers the phase shifts are continuous, i. e., $\theta_{n_\ell} \in [0, 2\pi)$, namely *RNN-based method with continuous phase shift* in our simulations. In order to fairly compare the proposed RAPL with the benchmark, we round the obtained continuous solutions to the discrete set, i.e., Φ_{K_ℓ}, namely, *RNN-based method with discrete phase shift*.
- ***DNN-based method*:** This is a DNN-based active sensing method proposed in [33]. This approach also assumes that the phase shifts are continuous, i. e., $\theta_{n_\ell} \in [0, 2\pi)$, namely *DNN-based method with continuous phase shift*.

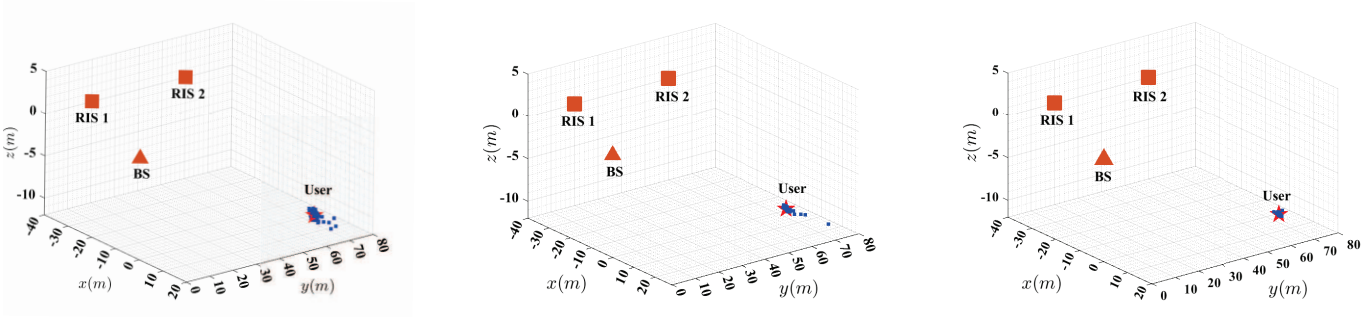

(a) $N \times \log N$ (b) $N^2 \times \log N$ (c) $N^3 \times \log N$

Fig. 5: Visual localization results for double-RIS network with different sample sizes.

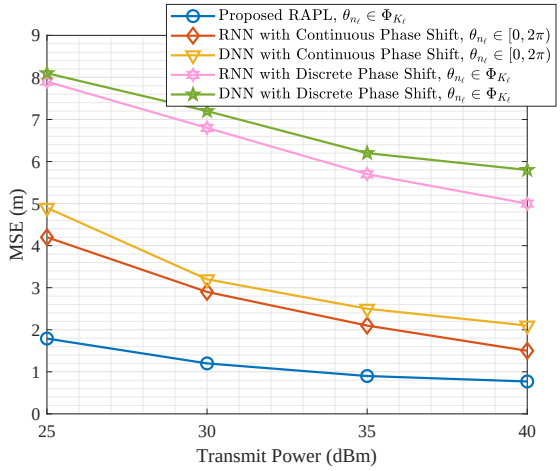

Fig. 6: Localization accuracy vs. transmit power in double-RIS MISO network with cascaded channel, $N = 64$, $M = 8$.

And we also round the obtained continuous solutions to the discrete set Φ_{K_ℓ} in our simulations, namely, *DNN-based method with discrete phase shift*.

It is noted that the RNN-based method updates the reflective coefficients based on the observed received signal strength and the reflective coefficients of the RISs in the previous time slot. In contrast, the DNN-based method updates the reflective coefficients according to the channel distribution to minimize the loss function.

The learning-based methods require retraining the neural network when the number of RISs increasing. [33] only shows the numerical results of a double-RIS case. Thus, when $L > 2$, we only compare the performance of proposed RAPL in different number of RISs.

B. Simulation Results

Fig. 3 shows the localization accuracy of different methods as the uplink transmit power varies without cascaded channels. For the proposed RAPL, the number of samples used in each experiment is $T = 2N^2 \times \log N$, while the learning-based methods are trained with $2,048,000$ samples and use $T = 6$ sets of pilots and phase shift samples in each experiment. It is clear that the proposed RAPL significantly outperforms the learning-based methods in terms of localization accuracy, even with fewer samples. In the case of continuous phase shifts, the MSE of the RNN-based method only converges to around 0.2, whereas the proposed RAPL can achieve an accuracy in the order of 10^{-3}. Moreover, it is also evident that under discrete phase shifts, the performance of the learning-based method drops significantly, far below that of the proposed RAPL.

Fig. 4 compares the performance of the proposed RAPL with the learning-based method under different training sample sizes. It is clear that when the training sample size is very small, the performance of the learning-based methods is poor, with localization accuracy significantly lower than that of the proposed RAPL. For instance, when the sample size is $N^3 \times \log N$, the localization MSE of the proposed RAPL is 0.0078, whereas the MSE of all other methods exceeds 1. When the sample size increases to 2048000, as used in [33], the MSE of the proposed RAPL can reach the order of 10^{-5}, which is still superior to the learning-based method. Moreover, Fig. 5 shows the visual localization results for double-RIS network with different sample sizes. We take a total of 1000 independent experiments and show every estimated position of the user in the 3D-coordinate. It can be observed that the estimated positions of the user are more and more concerted on the ground truth which is marked as a red star in the figure with the increasing of the sample size.

We only consider the parallel topology case in the above two simulations. We then compare the proposed RAPL with benchmarks in the cascade topology case. Note that the RNN-based method and DNN-based method both ignore the cascade channels, we here train the neural networks based on the no cascaded channel model, and test the localization performance with the cascaded channel model which is much closer to the real environment. The simulation result is shown in Fig. 6, we observe that the proposed RAPL significantly outperforms the learning-based methods with discrete phase shift. Even the proposed RAPL works better than the continuous solutions obtained by the learning-based methods.

Remark 1 (Discrete Phase shifts): As mentioned in (1), the proposed RAPL assumes that the phase shifts can be only selected from a finite discrete set, which better aligns with hardware constraints. However, the learning-based methods proposed in [33] assume the continuous phase shifts. We observe that when the continuous phase shift values are rounded to the discrete set, the learning-based methods exhibit

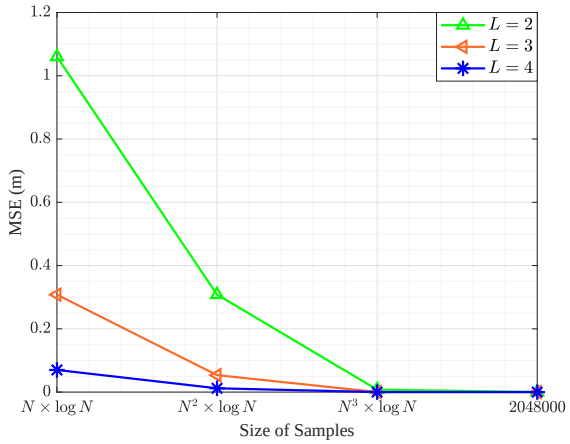

Fig. 7: Localization accuracy vs. size of samples in different number of RISs.

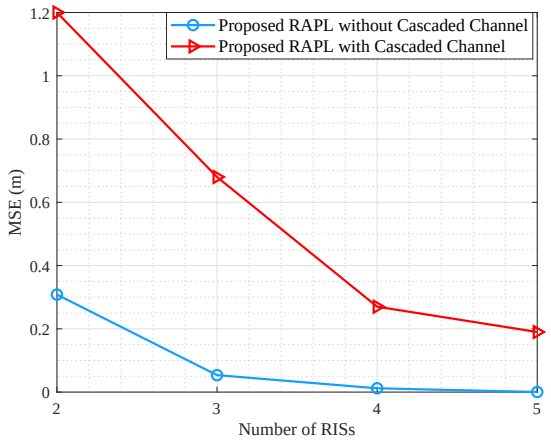

Fig. 8: Localization accuracy vs. number of RISs in different channel models.

poor performance in Fig. 3, Fig. 4 and Fig. 6.

Fig. 7 shows that with the increasing of number of RISs results when different sample size for all RISs are considered. We observe that with the increasing of number of RISs, the estimated positions become more accurate. And we also observe that no matter how the number of RISs changes, the positioning accuracy will significantly decrease as the sample size increases. Moreover, when the sample size reaches $N^3 \log N$, the localization error becomes less than 10^{-3} m, making the error sufficiently small.

Fig. 8 shows the localization accuracy versus the number of RISs in different channel models. It can be clearly seen that with the absence of cascaded channels, the positioning accuracy of proposed RAPL is significantly better compared to the case where cascaded channels are assumed. This is because the presence of cascaded channels introduces more cross terms in the channel model, making it more challenging to recover direction pairs. Additionally, neglecting some weaker cascaded channels also lead to additional errors. We also observe that in the presence of cascaded channels, the improvement of positioning accuracy with the increasing of the number of RISs when $L > 3$, is not significant. This is because, although the process of pinpointing the user's location using AoD pairs becomes more precise as the number of RIS increases, the accuracy of estimating the AoD pairs themselves decreases due to the presence of cascaded channels.

Remark 2 (Without Retraining): The proposed RAPL can be directly adapted to changes in the number of RISs or even an increase in the number of BSs. In contrast, the learning-based method proposed in [33] requires retraining the neural network when the number of RISs or BSs changes, leading to significant additional computational and time overhead.

VI. Conclusion

This paper proposes a data-driven multiple RISs-assisted passive localization, namely RAPL, with zero-overhead. The method first estimates phase differences between direct and reflected channels by utilizing the conditional sample mean approach, and then recovers the AoD pairs w.r.t each RIS to the user. With the estimated AoD pairs, we finally pinpoint the user position. The two distinct RIS topologies: the parallel topology and the cascaded topology, are both considered. These two cases offer greater generalizability compared to existing localization methods. Numerical results show that the proposed RAPL achieves higher localization accuracy with less sample size compared to the traditional methods. In addition, the proposed RAPL can circumvent the issues of the traditional methods that the need for CSI acquisition, communication interruptions, strong interactions between the RISs and the BS, and the requirement for large amounts of training data, showing its potential in practical deployments in future IoT and different edge networks.

References

[1] R. Di Taranto, S. Muppirisetty, R. Raulefs, D. Slock, T. Svensson, and H. Wymeersch, "Location-aware communications for 5G networks: How location information can improve scalability, latency, and robustness of 5G," *IEEE Signal Process. Mag.*, vol. 31, no. 6, pp. 102–112, Oct. 2014.

[2] D. Wei, L. Cao, L. Zhang, X. Gao, and H. Yin, "Non-primary channel access in IEEE 802.11 UHR: Comprehensive analysis and evaluation," in *Proc. IEEE Veh. Technol. Conf. (VTC fall)*, Washington, DC, USA, Oct. 2024, pp. 1–6.

[3] Y. Gu, A. Lo, and I. Niemegeers, "A survey of indoor positioning systems for wireless personal networks," *IEEE Commun. Surveys Tuts.*, vol. 11, no. 1, pp. 13–32, Mar. 2009.

[4] E. Y. Menta, N. Malm, R. Jäntti, K. Ruttik, M. Costa, and K. Leppänen, "On the performance of AoA–based localization in 5G ultra–dense networks," *IEEE Access*, vol. 7, pp. 33 870–33 880, Mar. 2019.

[5] N. Garcia, H. Wymeersch, E. G. Larsson, A. M. Haimovich, and M. Coulon, "Direct localization for massive MIMO," *IEEE Trans. Signal Process.*, vol. 65, no. 10, pp. 2475–2487, May 2017.

[6] X. Zhou, X. Du, and Y. Mao, "Cramér-rao bound based waveform optimization for MIMO radar: An efficient linear-proximal method," Sep. 2024, [Online]. Available https://arxiv.org/abs/2106.07065.

[7] C. L. Nguyen, O. Georgiou, G. Gradoni, and M. Di Renzo, "Wireless fingerprinting localization in smart environments using reconfigurable intelligent surfaces," *IEEE Access*, vol. 9, pp. 135 526–135 541, Sep. 2021.

[8] Q. Wu and R. Zhang, "Intelligent reflecting surface enhanced wireless network via joint active and passive beamforming," *IEEE Trans. Wireless Commun.*, vol. 18, no. 11, pp. 5394–5409, Nov. 2019.

[9] ——, "Beamforming optimization for wireless network aided by intelligent reflecting surface with discrete phase shifts," *IEEE Transactions on Communications*, vol. 68, no. 3, pp. 1838–1851, 2020.

[10] ——, "Towards smart and reconfigurable environment: Intelligent reflecting surface aided wireless network," *IEEE Commun. Mag.*, vol. 58, no. 1, pp. 106–112, Nov. 2020.

[11] C. Pan, H. Ren, K. Wang, J. F. Kolb, M. Elkashlan, M. Chen, M. Di Renzo, Y. Hao, J. Wang, A. L. Swindlehurst, X. You, and L. Hanzo, "Reconfigurable intelligent surfaces for 6G systems: Principles, applications, and research directions," *IEEE Commun. Mag.*, vol. 59, no. 6, pp. 14–20, Jul. 2021.

[12] C. Pan, G. Zhou, K. Zhi, S. Hong, T. Wu, Y. Pan, H. Ren, M. D. Renzo, A. Lee Swindlehurst, R. Zhang, and A. Y. Zhang, "An overview of signal processing techniques for RIS/IRS-aided wireless systems," *IEEE J. Sel. Topics Signal Process.*, vol. 16, no. 5, pp. 883–917, Aug. 2022.

[13] Z. Wang, X. Hu, C. Liu, and M. Peng, "RIS-enabled multi-target sensing: Performance analysis and space-time beamforming design," *IEEE Trans. Wireless Commun.*, vol. 23, no. 10, pp. 13 889–13 903, Oct. 2024.

[14] J. Li, S. Zhang, Z. Li, J. Ma, and O. A. Dobre, "User sensing in RIS-aided wideband mmwave system with beam-squint and beam-split," *IEEE Trans. Commun.*, pp. 1–1, 2024.

[15] X. Song, J. Xu, F. Liu, T. X. Han, and Y. C. Eldar, "Intelligent reflecting surface enabled sensing: Cramér-rao bound optimization," *IEEE Trans. Signal Process.*, vol. 71, pp. 2011–2026, May 2023.

[16] H. Zhang, H. Zhang, B. Di, K. Bian, Z. Han, and L. Song, "Towards ubiquitous positioning by leveraging reconfigurable intelligent surface," *IEEE Commun. Lett.*, vol. 25, no. 1, pp. 284–288, Jan. 2021.

[17] P. Wang, W. Mei, J. Fang, and R. Zhang, "Target-mounted intelligent reflecting surface for joint location and orientation estimation," *IEEE J. Sel. Areas Commun.*, vol. 41, no. 12, pp. 3768–3782, Oct. 2023.

[18] X. Song, D. Zhao, H. Hua, T. X. Han, X. Yang, and J. Xu, "Joint transmit and reflective beamforming for IRS-assisted integrated sensing and communication," in *Proc. IEEE Wireless Commun. Netw. Conf. (WCNC)*, Austin, TX, USA, Apr. 2022, pp. 189–194.

[19] J. Zhang, J. Tang, W. Feng, X. Y. Zhang, D. K. C. So, K.-K. Wong, and J. A. Chambers, "Throughput maximization for RIS-assisted UAV-enabled WPCN," *IEEE Access*, vol. 12, pp. 13 418–13 430, Jan. 2024.

[20] S. Gong, S. Ma, Z. Yang, C. Xing, and J. An, "Throughput maximization for asynchronous RIS-aided hybrid powered communication networks," *IEEE Trans. Wireless Commun.*, vol. 21, no. 6, pp. 4114–4132, Nov. 2022.

[21] S. Lin, Y. Zou, and D. W. K. Ng, "Ergodic throughput maximization for RIS-equipped-UAV-enabled wireless powered communications with outdated CSI," *IEEE Trans. Commun.*, vol. 72, no. 6, pp. 3634–3650, Jan. 2024.

[22] F. Xu, J. Yao, W. Lai, K. Shen, X. Li, X. Chen, and Z.-Q. Luo, "Blind beamforming for coverage enhancement with intelligent reflecting surface," *IEEE Trans. Wireless Commun.*, vol. 23, no. 11, pp. 15 736–15 752, Jul. 2024.

[23] W. Ma, L. Zhu, and R. Zhang, "Passive beamforming for 3-D coverage in IRS-assisted communications," *IEEE Wireless Commun. Lett.*, vol. 11, no. 8, pp. 1763–1767, Aug. 2022.

[24] T. Dhruvakumar and A. Chaturvedi, "Intelligent reflecting surface assisted millimeter wave communication for achievable rate and coverage enhancement," *Veh. Commun.*, vol. 33, p. 100431, Jan. 2022.

[25] M. A. Javed, T. N. Nguyen, J. Mirza, J. Ahmed, and B. Ali, "Reliable communications for cybertwin-driven 6G IoVs using intelligent reflecting surfaces," *IEEE Trans. Industr. Inform.*, vol. 18, no. 11, pp. 7454–7462, Nov. 2022.

[26] S. Lin, Y. Zou, B. Li, and T. Wu, "Security-reliability trade-off analysis of RIS-aided multiuser communications," *IEEE Trans. Veh. Technol.*, vol. 72, no. 5, pp. 6225–6237, May 2023.

[27] M. Zhou, F. Wu, K. Wang, Y. Sun, L. Liu, S. Mumtaz, M. Guizani, and D. Niyato, "Reliability enhancement for V2V communications: via af relay versus via passive RIS," *IEEE Trans. Commun.*, pp. 1–1, 2024.

[28] D. Zhou, S. Gong, L. Li, B. Gu, and M. Guizani, "Deep reinforcement learning for IRS-assisted secure NOMA transmissions against eavesdroppers," in *Proc. Int. Wireless Commun. Mobile Comput. (IWCMC)*, Ayia Napa, Cyprus, May 2024, pp. 1236–1241.

[29] M. Saif and S. Valaee, "Improving connectivity of RIS-assisted UAV networks using RIS partitioning and deployment," in *Proc. IEEE Veh. Technol. Conf. (VTC fall)*, Washington, DC, USA, Oct. 2024, pp. 1–6.

[30] W. Mei, B. Zheng, C. You, and R. Zhang, "Intelligent reflecting surface-aided wireless networks: From single-reflection to multireflection design and optimization," *Proc. IEEE*, vol. 110, no. 9, pp. 1380–1400, Sep. 2022.

[31] Z. Zhang, Y. Cui, F. Yang, and L. Ding, "Analysis and optimization of outage probability in multi-intelligent reflecting surface-assisted systems," Sep. 2019, [Online]. Available: https://arxiv.org/abs/1909.02193.

[32] F. Xu, J. Yao, W. Lai, K. Shen, X. Li, X. Chen, and Z.-Q. Luo, "Coordinating multiple intelligent reflecting surfaces without channel information," *IEEE Trans. Signal Process.*, vol. 72, pp. 31–46, Nov. 2023.

[33] Z. Zhang, T. Jiang, and W. Yu, "Localization with reconfigurable intelligent surface: An active sensing approach," *IEEE Trans. Wireless Commun.*, vol. 23, no. 7, pp. 7698–7711, Jul. 2024.

[34] Q. Li, K. Huang, Z. Deng, Z. Wan, and M. Yi, "A multi-RIS-assisted static environment sensing method," *IEEE Commun. Lett.*, vol. 28, no. 6, pp. 1317–1321, Jun. 2024.

[35] Z. Esmaeilbeig, K. V. Mishra, A. Eamaz, and M. Soltanalian, "Cramér-Rao lower bound optimization for hidden moving target sensing via multi-IRS-aided radar," *IEEE Signal Process. Lett.*, vol. 29, pp. 2422–2426, Nov. 2022.

[36] R. Liu, M. Li, Q. Liu, and A. Lee Swindlehurst, "SNR/CRB-constrained joint beamforming and reflection designs for RIS-ISAC systems," *IEEE Trans. Wireless Commun.*, vol. 23, no. 7, pp. 7456–7470, Jul. 2024.

[37] Y. Fang, S. Zhang, X. Li, X. Yu, J. Xu, and S. Cui, "Multi-IRS-enabled integrated sensing and communications," *IEEE Trans. Commun.*, vol. 72, no. 9, pp. 5853–5867, Sep. 2024.

[38] K. Chen and Y. Mao, "Transmitter side beyond-diagonal RIS for mmwave integrated sensing and communications," in *Proc. IEEE Int. Workshop Signal Process. Adv. Wireless Commun. (SPAWC)*, Lucca, Italy, Oct. 2024, pp. 951–955.

[39] A. Elzanaty, A. Guerra, F. Guidi, and M.-S. Alouini, "Reconfigurable intelligent surfaces for localization: Position and orientation error bounds," *IEEE Trans. Signal Process.*, vol. 69, pp. 5386–5402, Aug. 2021.

[40] X. Shao, C. You, W. Ma, X. Chen, and R. Zhang, "Target sensing with intelligent reflecting surface: Architecture and performance," *IEEE J. Sel. Areas Commun.*, vol. 40, no. 7, pp. 2070–2084, Jul. 2022.

[41] H. Luo, R. Liu, M. Li, Y. Liu, and Q. Liu, "Joint beamforming design for RIS-assisted integrated sensing and communication systems," *IEEE Trans. Veh. Technol.*, vol. 71, no. 12, pp. 13 393–13 397, Dec. 2022.

[42] B. Zheng, C. You, and R. Zhang, "Efficient channel estimation for double-IRS aided multi-user MIMO system," *IEEE Trans. Commun.*, vol. 69, no. 6, pp. 3818–3832, Jun. 2021.

[43] S. Bazzi and W. Xu, "IRS parameter optimization for channel estimation MSE minimization in double-IRS aided systems," *IEEE Wireless Commun. Lett.*, vol. 11, no. 10, pp. 2170–2174, Oct. 2022.

[44] C. You, B. Zheng, and R. Zhang, "Wireless communication via double IRS: Channel estimation and passive beamforming designs," *IEEE Wireless Commun. Lett.*, vol. 10, no. 2, pp. 431–435, Feb. 2021.

[45] K. Keykhosravi and H. Wymeersch, "Multi-RIS discrete-phase encoding for interpath-interference-free channel estimation," Apr. 2021, [Online]. Available https://arxiv.org/abs/2106.07065.

[46] X. Zheng, P. Wang, J. Fang, and H. Li, "Compressed channel estimation for IRS-assisted millimeter wave OFDM systems: A low-rank tensor decomposition-based approach," *IEEE Wireless Commun. Lett.*, vol. 11, no. 6, pp. 1258–1262, Mar. 2022.

[47] T. Jiang and W. Yu, "Active sensing for reciprocal MIMO channels," *IEEE Trans. Signal Process.*, vol. 72, pp. 2905–2920, Jun. 2024.

[48] Y. Li and W. Yu, "Localization in multipath environments via active sensing with reconfigurable intelligent surfaces," *IEEE Commun. Lett.*, vol. 28, no. 9, pp. 2061–2065, Jul. 2024.

[49] Z. Zhang and W. Yu, "Codebook learning for active sensing with reconfigurable intelligent surface," in *Proc. IEEE Int. Workshop Signal Process. Adv. Wireless Commun. (SPAWC)*, Lucca, Italy, Oct. 2024, pp. 821–825.

[50] Z. Zhang, T. Jiang, and W. Yu, "Active sensing for localization with reconfigurable intelligent surface," in *Proc. IEEE Int. Commun. Conf. (ICC)*, 2023, pp. 4261–4266.

[51] S. Ren, K. Shen, Y. Zhang, X. Li, X. Chen, and Z.-Q. Luo, "Configuring intelligent reflecting surface with performance guarantees: Blind beamforming," *IEEE Trans. Wireless Commun.*, vol. 22, no. 5, pp. 3355–3370, May 2023.

[52] J. Yao, F. Xu, W. Lai, K. Shen, X. Li, X. Chen, and Z.-Q. Luo, "Blind beamforming for multiple intelligent reflecting surfaces," in *Proc. IEEE Int. Commun. Conf. (ICC)*, Rome, Italy, May 2023.

[53] W. Lai, W. Wang, F. Xu, X. Li, S. Niu, and K. Shen, "Adaptive blind beamforming for intelligent surface," *IEEE Trans. Mobile Comput.*, pp. 1–17, 2024.

[54] V. Arun and H. Balakrishnan, "RFocus: beamforming using thousands of passive antennas," in *USENIX Symp. Netw. Sys. Design Implementation (NSDI)*, Feb. 2020, pp. 1047–1061.